Soft Matter

Accepted Manuscript

ROYAL SOCIETY OF CHEMISTRY

www.rsc.org/softmatter

In situ Measurement of Contact Angle and Surface Tension of Interfacial Nanobubbles in Ethanol Aqueous Solutions

Binyu Zhao,[abc] Xingya Wang,[acd] Shuo Wang,[ac] Renzhong Tai,[acd] Lijuan Zhang*[acd,] and Jun Hu*[ac]

[a] Shanghai Institute of Applied Physics, Chinese Academy of Sciences, Shanghai 201800, China
[b] School of Mechanics and Engineering, Southwest Jiaotong University, Chengdu 610031, China
[c] Key Laboratory of Interfacial Physics and Technology, Chinese Academy of Sciences, Shanghai 201800, China
[d] Shanghai Synchrotron Radiation Facility, Shanghai 201204, China

*Correspondence to [zhanglijuan@sinap.ac.cn] or [hujun@sinap.ac.cn]

Abstract

The astonishing long lifetime and large contact angles of interfacial nanobubbles are still in hot debates despite of numerous experimental and theoretical studies. One hypothesis to reconcile the two abnormalities of interfacial nanobubbles is that they had low surface tensions. However, few studies have been done to measure the surface tensions of nanobubbles due to the lack of effective measurements. Here, we investigated the *in situ* contact angles and surface tensions of individual interfacial nanobubbles immersed in different ethanol aqueous solutions by quantitative nanomechanical atomic force microscopy (AFM). Results showed that the contact angles of nanobubbles in the studied ethanol solutions were also much larger than the corresponding macroscopic counterparts on the same substrate, and they decreased with the increasing ethanol concentrations. More significantly, the surface tensions calculated were much lower than those of the gas-liquid interfaces of the solutions at macroscopic scale but have the similar tendency with the increasing ethanol concentrations. Those results are expected to further understand the stability of interfacial nanobubbles in complex solutions.

Introduction

Nanoscale gas bubbles attached at the solid surfaces immersed in water, known as interfacial nanobubbles or surface nanobubbles,[1-6] were originally invoked to explain the long range attractive force between hydrophobic surfaces in water,[7] and then directly been observed by tapping mode atomic force microscopy (TM-AFM) imaging.[8-10] They have far reaching potential implications in a range of interfacial phenomena and technical applications, such as the long range attraction between hydrophobic surfaces in solutions,[7, 11] the stability of colloids and emulsions,[12, 13] interfacial slippage in microfluidics,[14-16] froth flotation and mineral separation,[17, 18] and bio-molecular adsorption.[19, 20] However, classical thermodynamics predicts that such small bubbles should dissolve in less than a few hundred microseconds.[21, 22]

To date, a large number of studies have focused on the confirmation of the existence of interfacial nanobubbles and the mechanism for their superstability. Their existence and gaseous nature have been confirmed by the pre-degassing and post-degassing experiments,[23, 24] electrochemical method,[25, 26] spectroscopy,[27] imaging by optical,[28-31] electron,[32, 33] X-ray[34] microscopy and many other techniques.[6] The explanation of stability such as line tension,[35] contamination,[36, 37] high density,[38] dynamic equilibrium,[39] Knudsen gas,[40] and gas layer,[41] have been proposed to understand the superstability of nanobubbles, but none of them could give an uncontested explanation. Recent findings have showed that the nanobubble-liquid-substrate three phase contact line was pinned,[42-44] both the contact line pinning and gas supersaturation are very crucial for the long lifetime of interfacial nanobubbles, as well as for the large contact angle.[45, 46]

The contact angle and surface tension of the liquid/gas interface of nanobubbles are two most important properties for interfacial nanobubbles. Zhang *et al.* investigated the wetting phenomena of a droplet of ethanol/water solution on graphite with varied surface tensions as well as contact angles by simply changing the concentrations of the ethanol solutions.[47] However, it is still a difficulty to obtain the contact angle and the surface tension simultaneously at nanometer scale. While the contact angles of nanobubbles were commonly obtained from their geometry in AFM images,[48-50] the measurement of the surface tensions of nanobubbles has long been a challenge. From Young-Laplace equation, if the surface tension was decreased, the pressure inside nanobubble would be

lowered. Surface tension is the driving force for nanobubble dissolution. A lower surface tension decreases the Laplace pressure, thus decreasing the driving that leads to dissolution. Previously, interfacial nanobubbles in water, surfactant solutions, or non-aqueous solutions have been shown with low spring constants (stiffness) measured by FV mode AFM, comparing well with the literature surface tension values of the liquids at the same concentration.[51-54] Our recent PeakForce Quantitative Nano-Mechanics (PF-QNM) measurement also showed that the stiffness of nanobubbles in pure water was close to the surface tension of water.[55] However, the stiffness cannot be simply equal to surface tension. Attard *et al.* have worked out two quantitative relationships between the stiffness and surface tension of small gas bubbles,[56-58] which can be used for references to describe the correlation between the surface tension and stiffness of nanobubbles. And very recently, Attard claimed that the surface tension of nanobubbles was 40-50 mN/m in pure water.[58] However, it was limited to measure nanobubbles only in water. The systematical study of surface tensions of nanobubbles in varied solution is still scarce. Moreover, it is more significant to investigate how the contact angles and surface tensions of nanobubbles will change in solutions with continuously tuned surface tensions in order to understand the stability of nanobubbles.

PF-QNM is a direct force control mode AFM that make the measurement of force at each pixel precisely, allowing one to control and minimize the force between the tip and sample, and the corresponding force curves can be extracted automatically from which the stiffness is extracted at each pixel. So, the mechanical properties can be directly quantified simultaneously with the topographical imaging with high resolution.[55, 59-62] In this study, we used ethanol to tune the surface tension of the liquids around nanobubbles so as to investigate the surface tension effects on the properties and stability of interfacial nanobubbles in ethanol aqueous solutions. The *in situ* contact angles and surface tensions of interfacial nanobubbles in ethanol aqueous solutions with different concentrations were measured using PF-QNM. Results showed that the contact angles of nanobubbles were much larger than those of macrodroplets not only in water but also in ethanol solutions. More interestingly, the surface tensions of nanobubbles reduced while the ethanol concentration increased accordingly. Those results are helpful to understand the stability of nanobubbles in more complex solution environment.

Experimental section

1. Materials

Highly Ordered Pyrolytic Graphite (HOPG, ZYB grade, NT-MDT, Russia) with a water contact angle of 68 ± 4° was freshly cleaved and used as substrate. Ultra-pure water with a conductivity of 18.2 MΩ•cm was prepared by a USF-ELGA Maxima water purification system. Ethanol (≥99.8%, GR) was purchased from Sinopharm Chemical Reagent Co., Ltd. The ethanol aqueous solutions with concentration of 0%, 10%, 20%, 30%, 40%, 50%, and 60% in volume were prepared respectively. These solutions was prepared in lidded glass bottles (ultrasonic cleaned by water, ethanol, and water again, and were extensively rinsed by pure water) and shocked for 5min for air equilibrium. The AFM used here was Bruker's Multimode SPM equipped with NanoScope 8.15 Software and NanoScope V Controller. Silicon nitride tip with cantilever (NPS, 0.35N/m, 10nm tip radius, Bruker) was treated by Plasma Cleaner (HARRICK PLASMA, PLASMA CLEANER PDC-32G) for 1-2 minutes beforehand and used immediately to avoid contamination.

2. Nanobubbles production

The quartz liquid cell, silicone tubes and silicone O-ring provided by Bruker, and sterile syringes with 5mL volume purchased from Sinopharm Chemical Reagent Co., Ltd. were extensively rinsed with ethanol and water in turn. The plasma treated probe was loaded on the assembled liquid cell and then put on the freshly cleaved HOPG substrate. The cleaned syringes were used to extract liquids. Nanobubbles were prepared on the freshly cleaved HOPG surface by the popularly used ethanol-water exchange procedure as it was easily operated and could produce nanobubbles repeatedly.[8, 53] Main steps as followed: water was injected firstly into the liquid cell. Then, ethanol was injected to displace the water. Finally, interfacial nanobubbles appeared on the surface after the ethanol was exchanged by water.

3. PF-QNM imaging

After the ethanol-water exchange, nanobubbles were first imaged in pure water, after which 5mL 10% ethanol aqueous solution was carefully injected to replace the pure water in the liquid cell, and the same area was imaged again. Then 5mL 20% ethanol aqueous solution was injected to replace the 10% ethanol aqueous solution and *in situ* image was

captured. In turn, low concentration ethanol solution was replaced by a higher concentration ethanol solution. About 5mL solution was efficient to displace the original solution in the liquid cell (~100 μL) as 4-6 mL water was tested to make an efficient displacement of ~500μL ethanol.[63] We usually waited for about 10 minutes for system equilibration and then captured *in situ* the corresponding topography and stiffness images after each replacement. The deflection sensitivity and spring constant for each cantilever were measured using the built-in cantilever calibration, ramp and thermal noise method, respectively. The peakforce amplitude was set at 100nm, peakforce frequency at 2 kHz and scan rate at 0.977Hz. The peakforce setpoint was carefully set at a loading force (100pN ~ 400pN) as smaller as possible considering the very soft and fragile features of nanobubbles. All AFM experiments were performed in a closed liquid cell configuration with an O-ring at room temperature (~25□). The AFM offline processing system, NanoScope Analysis software, was used for morphology and stiffness values measurements and analysis.

4. Macroscopic contact angles measurement

The macroscopic contact angles of ethanol solutions on HOPG substrate were measured on an Attension Theta system (KSV Instruments Ltd., Finland). A digital camera with supplied calibration software recorded the profile of the advancing droplet of 5μL solution that was dropped on the freshly cleaved HOPG surface, from which the contact angles were determined.

Results and discussion

1. *In situ* PF-QNM imaging of nanobubbles in ethanol/water solutions

It was reported that most of the nanobubbles were stable and could be imaged in ethanol aqueous solutions below 70%vol after formation.[64] Previously, we successfully used PF-QNM to simultaneously obtain the morphology and stiffness of nanobubbles in pure water.[55] Here, the morphology and stiffness images of nanobubbles immersed in different ethanol aqueous solutions from 0% to 60% were obtained *in situ* by using PF-QNM. Fig. 1 shows the height (a) and stiffness (b) images of nanobubbles on graphite surfaces immersed in different ethanol solutions. (Here only the ethanol concentrations of 0%,

20%, 40% and 60% are shown for examples (see Fig. S1 in the Supporting Information for other concentrations). Nanobubbles can be stably imaged in ethanol aqueous solutions after formation and most nanobubbles could exist there for hours with some changes in size, while a few of them moved, coalesced or disappeared sometimes with the increase of ethanol concentration. Hence, we were able to trace the changes on the heights, lateral widths and stiffness of individual nanobubbles *in situ* in ethanol solutions with different concentrations which lead to a continuously varied surface tension. As a typical example, the nanobubbles numbered from 1 to 10 will be used for further analysis in the following part.

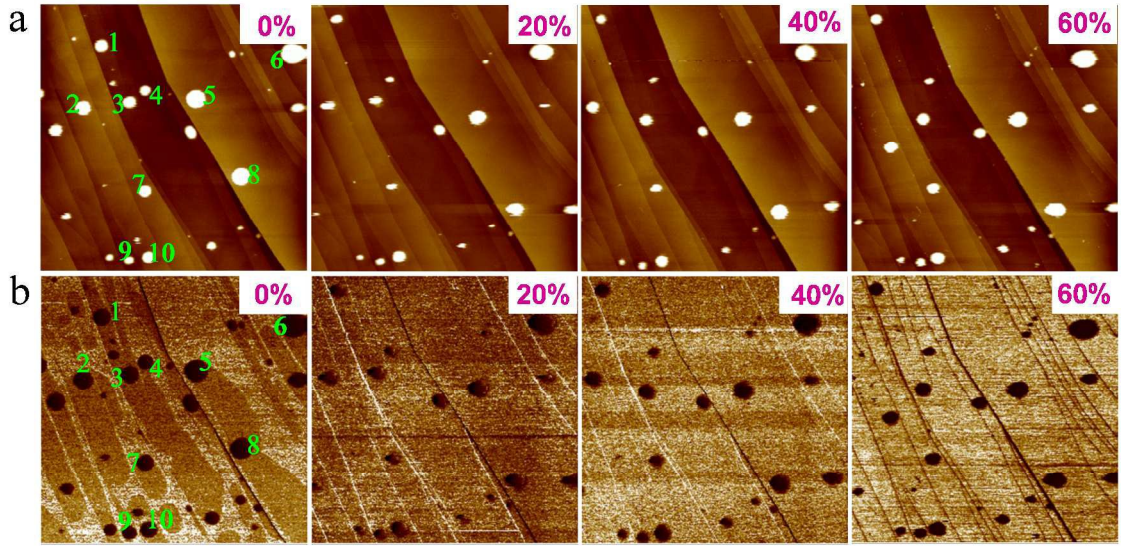

Fig. 1 Height (a) and stiffness (b) images of nanobubbles being immersed in ethanol aqueous solutions with different concentrations obtained by *in situ* PF-QNM. The ethanol concentrations (in vol %) were labeled in each image. Scan size 5μm×5μm. The nanobubbles numbered from 1 to 10 will be used for further analysis below.

2. *In situ* contact angles of nanobubbles in ethanol/water solutions

The contact angles of nanobubbles cannot be measured directly. Researchers in this field commonly determined the contact angles of nanobubbles from the nanobubbles' geometries obtained by AFM at imaging forces as low as possible, i.e. the heights and lateral widths of nanobubbles. Nanobubbles with lateral width larger than 100 nm were analyzed in our experiments to avoid the influence of the long-range van der Waals forces

on the contact angles measurements of nanobubbles.[65] Besides, as the AFM tip may be attracted to the nanobubble surface and deform it, the measured heights and lateral widths are subjected to corrections to exclude the force induced deformation and the tip size induced lateral extension of nanobubbles in order to obtain the contact angles as precise as possible. One of the advantages of PF-QNM mode AFM is that the force exerted at each pixel can be controlled precisely. So we were very careful to control the force during the imaging of nanobubbles. Here, we used the force of 100-400pN (depending on the solution in which the image was captured), the smallest force for stable imaging. Under such small loading forces, PF-QNM mode has been found to give out the comparable morphology of nanobubbles with tapping mode AFM[49, 55, 61].

We analyzed the changes of the geometries of ten typical nanobubbles. As showed in Fig. 2, the *in situ* heights and lateral widths of the ten typical nanobubbles as a function of the ethanol concentration were plotted, respectively. These values are corrected results after having excluded the force induced deformation and the tip size induced lateral extension of nanobubbles.[66]

$$H=H_a+ F/k$$

$$R= [(W_a/2)^2 +H^2)]/2H-R_{tip}$$

$$W=2(2RH-H^2)^{0.5}$$

$$\theta=\cos^{-1}(H/R-1)/\pi\times180°$$

where H is the height after calibration, H_a is the measured apparent height, W is the lateral width after calibration, W_a is the measured apparent lateral width, R is the curvature radius after calibration, R_{tip} is the tip radius, F is the loaded force, k is the stiffness of nanobubbles, and θ is the contact angle (measured through the liquid side) of nanobubbles.

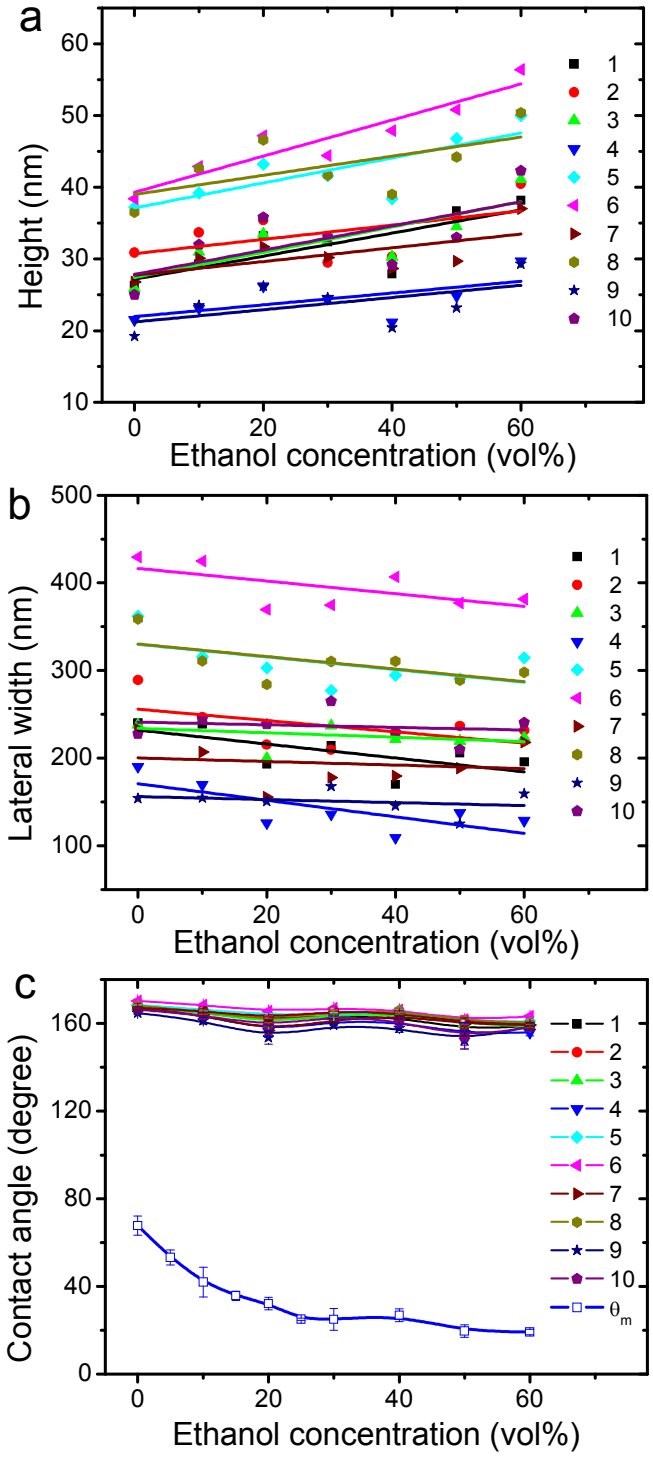

Fig. 2 Height (a), lateral width (b) and contact angles (c) of nanobubbles in ethanol/water solutions. In (c), the contact angles of macrodroplets (θ_m) of ethanol/water solutions were also plotted as a comparison.

It was found that the height increased and lateral width decreased slightly as the ethanol concentration increased. The contact angles of the ten typical nanobubbles were shown in Fig. 2c in comparison to those of macrodroplets (MDs). The contact angles of nanobubbles were much larger than the macroscopic measurements in water, in consistent with literature reports.[49, 53, 67] It was found that the contact angles of nanobubbles decreased from about 160° to 130° while the corresponding macroscopic contact angles decreased from about 70° to 20° as the ethanol concentration changed from 0% to 60%. The present study indicated that the contact angles of nanobubbles were also much larger than their macroscopic counterparts in different ethanol solutions, and they both decreased with the increase of the ethanol concentrations. Although their absolute value differed, the contact angles of the nanobubbles and the MDs showed a similar trend with the change of ethanol concentration, as seen from Fig. 2c.

Some recent works reported that the nanobubbles were pinned and the geometry which determines the contact angles,[42-44] i.e. the height and lateral width, may vary with ethanol concentrations. Ethanol solution of higher concentration with lower surface tension is easier to wet HOPG, and the effect of ethanol on nanobubbles might be enhanced by the enriched ethanol near the HOPG surface as the composition of ethanol-water solution is not usually uniform at the molecular level.[68] Therefore, the change of the nanobubble geometry might be mainly attributed to the decreasing of the surface tension as the evidence of the pinning effects appeared clearly once the width did not change when the height changed.[42-44] The addition of ethanol has been found to decrease the contact angle (at the liquid side) of hydrophobic surface in water, and decrease the long-range attraction and adhesion between hydrophobic surfaces in water.[7, 47, 69, 70]

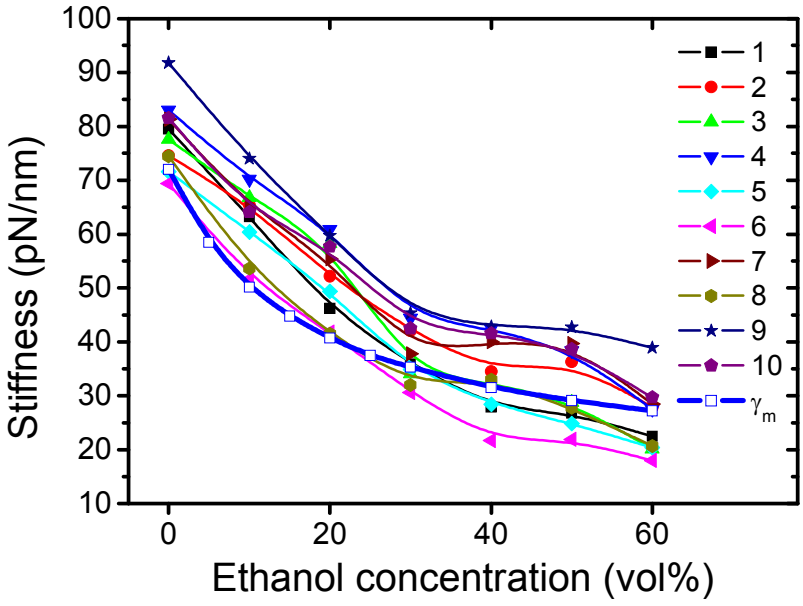

Fig. 3 Stiffness of nanobubbles versus the ethanol concentration of the solutions. The stiffness of 10 nanobubbles (named in numbers) *in situ* imaged in different ethanol solutions by PF-QNM were directly measured from the stiffness images. The surface tension of macrodroplets[71] (γ_m) were also showed for comparison.

3. *In situ* surface tension of nanobubbles in ethanol/water solutions

Fig. 3 shows the stiffness of nanobubbles marked in Fig. 1 in a series of ethanol solutions. The stiffness is calculated at each pixel of the image from the slope in the retraction trace of each oscillation cycle. To avoid the contribution of the long-range forces and adhesion, we restricted the fit to a range in between 10% and 70% of the force (peakforce + adhesion force) as reported in our pervious paper.[55] The stiffness of nanobubbles in pure water is very close to the surface tension of water, which is the same as the surface tension of micron-sized bubbles,[56] in consistent with our previous PF-QNM measurements[55] and very recent force volume measurements by Walczyk *et al.*[51, 52] In addition, Zhang *et al.* reported a stiffness of 43 mN/m of nanobubbles in Tween 20 solutions,[53] and An *et al.* reported a stiffness of 55 mN/m of nanobubbles in formamide,[54] both were comparable with the literature surface tension values of the liquids. Obviously, as the concentration of the ethanol aqueous solutions increased, the stiffness of

nanobubbles decreased. And the stiffness of nanobubbles was close to the surface tensions of the solutions at each studied ethanol concentration. However, the stiffness cannot be simply equal to surface tension. Attard *et al.* have worked out a quantitative correlation between the stiffness and surface tension of micron-sized gas bubbles (method 1).[56, 57] And very recently, a new model to calculate the surface tensions of nanobubbles based on the AFM force curves was also developed (method 2).[58] These two methods can be used to determine the surface tensions of nanobubbles from the corresponding stiffness.

Method 1:

$$k = -4\pi\gamma\left\{\frac{\cos\theta}{2+\cos\theta} + \ln\left[\frac{R_p}{2\kappa R_c^{\,2}}\frac{(1+\cos\theta)^2}{\sin^2\theta}\right]\right\}^{-1}.$$

Here k is the stiffness, γ is the surface tension of the liquid/vapor interface, θ is the gas-side contact angle, R_p is the tip radius, R_c is the bubbles' curvature radii, and κ^{-1} is the decay length for an exponentially decaying interaction pressure.

Method 2:

$$k = -2\pi\gamma\left[\frac{1}{2}\ln\frac{1-\sqrt{1-\left(\frac{r_1}{R_c}\right)^2}}{1+\sqrt{1-\left(\frac{r_1}{R_c}\right)^2}} + \frac{1}{\sqrt{1-\left(\frac{r_1}{R_c}\right)^2}} - \frac{1}{2}\ln\frac{1-\sqrt{1-\left(\frac{r_2}{R_c}\right)^2}}{1+\sqrt{1-\left(\frac{r_2}{R_c}\right)^2}} - \frac{1}{\sqrt{1-\left(\frac{r_2}{R_c}\right)^2}}\right]^{-1}.$$

Here r_1 is the radius of tip by which the nanobubble was penetrated and deformed; r_2 is the base radius of nanobubble which is it contact with the substrate, i.e., half of the lateral width of nanobubbles.

We used method 1 to extract the surface tensions of nanobubbles by directly measuring the stiffness of nanobubbles, and extended this method to nanobubbles in ethanol solutions. The results were shown in Fig. 4a. The surface tensions of nanobubbles in water are 20-30mN/m calculated based on this method. Clearly, the surface tensions of the nanobubbles are much lower than those of macrodroplets and they both decrease with increasing of the ethanol concentration.

It was indicated by Attard that when the nanobubble contact line was pinned to a

penetrating tip, the air-water interface of nanobubble behaved like a Hookean spring with spring constant proportional to the nanobubble surface tension. The AFM force curves data were analyzed and yielded nanobubble surface tension in the range of 40-50 mN/m.[58] Here, by using this method (method 2) we obtained the surface tensions of nanobubbles not only in water but also in ethanol solutions as shown in Fig. 4b. Unlike method 1 that was used to calculate the stiffness of micron-sized bubbles from their air-water surface tension, method 2 was used to measure the surface tension of nanobubbles from the AFM force curves. The surface tensions of nanobubbles in water were 30-40mN/m determined by method 2 in our experiments, which were much closer to those obtained by Attard. The small deviations should be due to the differences in supersaturation between that achieved by the ethanol-water exchange method and that previously equilibrating the water with air at a higher pressure or at a lower temperature.[3, 58] A higher supersaturation led to a lower surface tension.[3] As the ethanol concentration increased, the surface tensions of the nanobubbles were reduced and were much lower than those of macrodroplets.

As was shown above, we elucidated experimentally that the surface tensions of nanobubbles in water deduced from both methods were much lower than the surface tension of pure water, even though there were differences between the two results. The lower surface tensions of nanobubbles might be one of reason for their long lifetime. Interestingly, very weak size dependence behaviors of the surface tensions of nanobubbles were found in the low concentrated ethanol-water solutions where larger bubbles presented slightly larger surface tension. However, as the ethanol concentration increased, the surface tension has no evident size dependence as showed in the followed figure. The value of surface tension is within the error bar (see Fig. S2). The 30-40 mN/m surface tensions of nanobubbles obtained in our system are slightly lower than the reported 40-50 mN/m. The differences might be due to several factors, such as the different mode of AFM used, the tip wettability or shape, the variation of gas supersaturation, temperature, loading force, substrate contact line pinning, etc. But the results are consistent with reported that the nanobubble surface tension was less than the air-water surface tension. Furthermore, nanobubbles in ethanol solutions also showed lower surface tensions than those of macrodroplets of the same ethanol solutions.

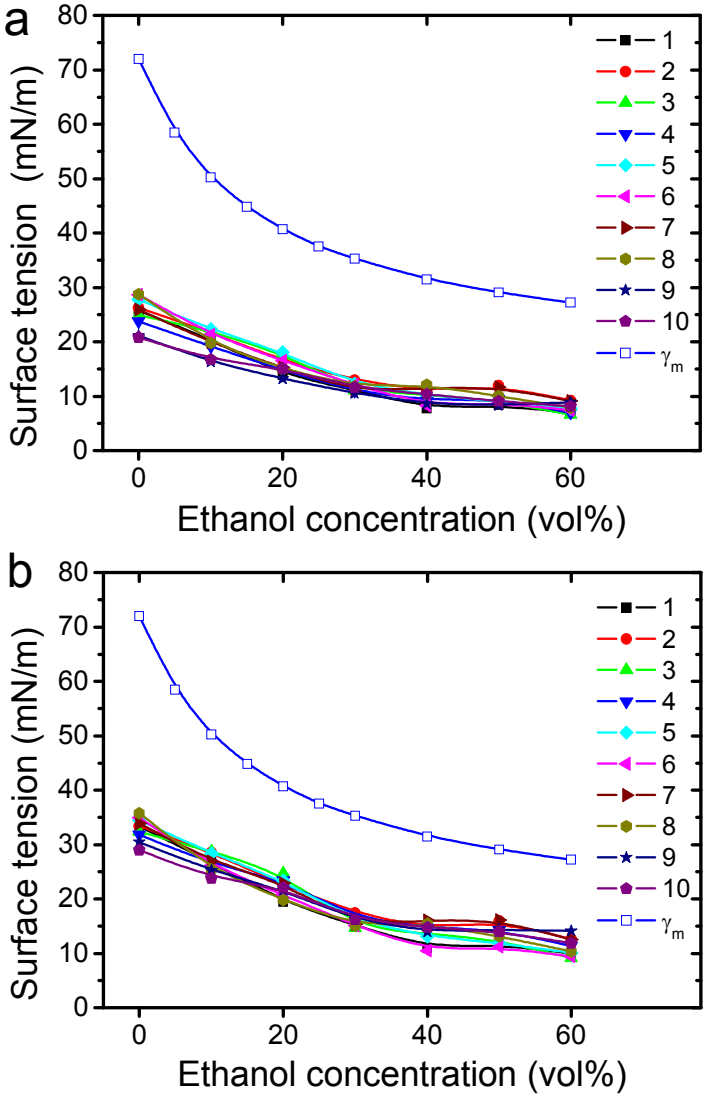

Fig. 4 Surface tension of nanobubbles versus the ethanol concentration of the solutions. The surface tensions of the 10 nanobubbles were calculated from their corresponding stiffness based on two different models. For method 1 (a), typical values of tip radius R_p=10nm and decay length κ^{-1}=10nm were used. For method 2 (b), $r_1=R_p$=10nm and r_2=W/2 were used. The surface tensions of macrodroplets (γ_m) were also showed for comparison.

So, how to explain that the surface tension of nanobubbles is lower than that of macrodroplets on the same surface? Previously, it was assumed that a film of contamination might cover on the nanobubbles surfaces so as to hinder the diffusion of gas and lower the surface tension which stabilizes the nanobubbles. [36, 72] But latter

experiments disproved the possibility that a film of contaminants could cover on the nanobubbles surfaces.[63] Recently, Berkelaar *et al.* reported that in some cases the AFM imaged nanobubble-like objects might be induced by PDMS contaminations.[73] However, when we imaged the surface first in water and then in ethanol, no objects were observed on the surface in our experiments (see Fig. S3). Nanobubbles were observed after the ethanol was exchanged by water again, and no residues were observed after removing the liquid and imaging the same area in water again (see Fig. S4). The above tests should exclude the possibility of PDMS contamination in our experiments. Therefore, the origin of low surface tension of nanobubbles is not clear. One of possible reasons might be due to the gas supersaturation near the nanobubbles interfaces as reported that a higher supersaturation leads to a lower surface tension.[3, 58, 74]

Conclusions

Interfacial nanobubbles were prepared on HOPG substrate immersed in ethanol-water solutions with different concentrations. By using PF-QNM mode AFM, both the morphology and the stiffness of nanobubbles were obtained *in situ*. As a result, we were able to investigate the contact angles and the surface tensions of the nanobubbles on a defined substrate as a function of ethanol concentrations. The results showed that the contact angles of nanobubbles were much larger than those of macrodroplets not only in water but also in ethanol solutions. The directly measured stiffness of nanobubbles in ethanol aqueous solutions was very close to the macroscale values, comparable to that of the nanobubbles in water, surfactant solutions and non-aqueous solutions measured by FV mode AFM. From the stiffness, the *in situ* surface tensions of nanobubbles were also derived from the corresponding stiffness on basis of two methods. Both methods exhibited that the surface tensions of nanobubbles were lower than those of their macroscale counterparts, in consistent with the recent FV mode AFM measurements. As the ethanol concentration increased, the surface tensions of nanobubbles reduced. The lower surface tension predicted is consistent with the notion of higher stability of nanobubbles. The present work should shed light on the future studies of the properties and stability of nanobubbles in non-aqueous solutions.

Acknowledgements

The authors thank the support from the Key Laboratory of Interfacial Physics and Technology, Chinese Academy of Sciences, and the Open Research Project of the Large Scientific Facility of the Chinese Academy of Sciences: Study on Self-assembly Technology and Nanometer Array with Ultra-high Density. We also thank the beamline 08U1A staffs at the Shanghai Synchrotron Radiation Facilities (SSRF) for the sample preparation and discussion. We gratefully acknowledge the generous financial support by the National Natural Science Foundation of China (Nos. 11079050, 11290165, 11305252, 11575281, U1532260), the National Basic Research Program of China (No. 2013CB932801), the National Natural Science Foundation for Outstanding Young Scientists (no. 11225527), the Shanghai Academic Leadership Program (no. 13XD1404400), 973 project (no. 2012CB825705), and the Knowledge Innovation Program of the Chinese Academy of Sciences (No. KJCX2-EW-W09, U1532260).

References

1. J. R. T. Seddon and D. Lohse, *Journal of Physics: Condensed Matter*, 2011, **23**, 133001.
2. V. S. J. Craig, *Soft Matter*, 2011, **7**, 40-48.
3. P. Attard, *Eur. Phys. J. Spec. Top.*, 2013, 1-22.
4. H. Peng, G. R. Birkett and A. V. Nguyen, *Adv Colloid Interfac*, 2015, **222**, 573-580.
5. H. J. An, G. M. Liu and V. S. J. Craig, *Adv Colloid Interfac*, 2015, **222**, 9-17.
6. D. Lohse and X. Zhang, *Reviews of Modern Physics*, 2015, **87**, 981-1035.
7. J. L. Parker, P. M. Claesson and P. Attard, *J Phys Chem-Us*, 1994, **98**, 8468-8480.
8. S.-T. Lou, Z.-Q. Ouyang, Y. Zhang, X.-J. Li, J. Hu, M.-Q. Li and F.-J. Yang, *Journal of Vacuum Science & Technology B: Microelectronics and Nanometer Structures*, 2000, **18**, 2573-2575.
9. N. Ishida, T. Inoue, M. Miyahara and K. Higashitani, *Langmuir*, 2000, **16**, 6377-6380.
10. J. W. G. Tyrrell and P. Attard, *Phys Rev Lett*, 2001, **87**, 176104.
11. M. A. Hampton and A. V. Nguyen, *Adv Colloid Interfac*, 2010, **154**, 30-55.
12. R. M. Pashley, *J. Phys. Chem. B*, 2003, **107**, 1714-1720.
13. R. M. Pashley, M. Rzechowicz, L. R. Pashley and M. J. Francis, *J Phys Chem B*, 2005, **109**, 1231-1238.
14. Y. Wang and B. Bhushan, *Soft Matter*, 2010, **6**, 29-66.
15. M. Abdelhamid and B. Bharat, *Journal of Physics: Condensed Matter*, 2013, **25**, 184003.
16. A. Finger and D. Johannsmann, *Phys Chem Chem Phys*, 2011, **13**, 18015-18022.
17. S. Heinrich, *International Journal of Mineral Processing*, 2005, **78**, 11-21.
18. S. Yang and A. Duisterwinkel, *Langmuir*, 2011, **27**, 11430-11435.
19. Z. H. Wu, X. H. Zhang, X. D. Zhang, G. Li, J. L. Sun, Y. Zhang, M. Q. Li and J. Hu, *Surface and Interface Analysis*, 2006, **38**, 990-995.
20. G. M. Liu and V. S. J. Craig, *Acs Appl Mater Inter*, 2009, **1**, 481-487.
21. P. S. Epstein and M. S. Plesset, *The Journal of Chemical Physics* 1950, **18**, 1505-1509.
22. S. Ljunggren and J. C. Eriksson, *Colloids and Surfaces A: Physicochemical and Engineering Aspects*, 1997, **129-130**, 151-155.

23. X. H. Zhang, X. D. Zhang, S. T. Lou, Z. X. Zhang, J. L. Sun and J. Hu, *Langmuir*, 2004, **20**, 3813-3815.
24. X. H. Zhang, G. Li, N. Maeda and J. Hu, *Langmuir*, 2006, **22**, 9238-9243.
25. L. Zhang, Y. Zhang, X. Zhang, Z. Li, G. Shen, M. Ye, C. Fan, H. Fang and J. Hu, *Langmuir*, 2006, **22**, 8109-8113.
26. S. Yang, P. Tsai, E. S. Kooij, A. Prosperetti, H. J. W. Zandvliet and D. Lohse, *Langmuir*, 2009, **25**, 1466-1474.
27. X. H. Zhang, A. Khan and W. A. Ducker, *Phys Rev Lett*, 2007, **98**, 136101.
28. C. U. Chan and C.-D. Ohl, *Phys Rev Lett*, 2012, **109**, 174501.
29. S. Karpitschka, E. Dietrich, J. R. T. Seddon, H. J. W. Zandvliet, D. Lohse and H. Riegler, *Phys Rev Lett*, 2012, **109**, 066102.
30. C. U. Chan, L. Chen, M. Arora and C.-D. Ohl, *Phys Rev Lett*, 2015, **114**, 114505.
31. D. Seo, S. R. German, T. L. Mega and W. A. Ducker, *J Phys Chem C*, 2015, **119**, 14262-14266.
32. E. R. White, M. Mecklenburg, S. B. Singer, S. Aloni and B. C. Regan, *Appl Phys Express*, 2011, **4** 055201.
33. D. Shin, J. B. Park, Y.-J. Kim, S. J. Kim, J. H. Kang, B. Lee, S.-P. Cho, B. H. Hong and K. S. Novoselov, *Nat Commun*, 2015, **6**, 6068.
34. L. Zhang, B. Zhao, L. Xue, Z. Guo, Y. Dong, H. Fang, R. Tai and J. Hu, *Journal of Synchrotron Radiation*, 2013, **20**, 413-418.
35. J. Yang, J. Duan, D. Fornasiero and J. Ralston, *The Journal of Physical Chemistry B*, 2003, **107**, 6139-6147.
36. W. A. Ducker, *Langmuir*, 2009, **25**, 8907-8910.
37. S. Das, *Phys Rev E*, 2011, **83**, 066315.
38. L. Zhang, H. Chen, Z. Li, H. Fang and J. Hu, *Science in China Series G: Physics, Mechanics & Astronomy*, 2008, **51**, 219-224.
39. M. P. Brenner and D. Lohse, *Phys Rev Lett*, 2008, **101**, 214505.
40. J. R. T. Seddon, H. J. W. Zandvlie and D. Lohse, *Physical Review Letters*, 2011, **107**, 116101.
41. H. Peng, M. A. Hampton and A. V. Nguyen, *Langmuir*, 2013, **29**, 6123-6130.
42. X. Zhang, D. Y. C. Chan, D. Wang and N. Maeda, *Langmuir*, 2013, **29**, 1017-1023.
43. Y. Liu and X. Zhang, *The Journal of Chemical Physics*, 2013, **138**, 014706.
44. J. H. Weijs and D. Lohse, *Physical Review Letters*, 2013, **110**, 054501.
45. Y. W. Liu and X. R. Zhang, *J Chem Phys*, 2014, **141**.
46. D. Lohse and X. Zhang, *Phys Rev E*, 2015, **91**, 031003.
47. X. Zhang, A. Kumar and P. J. Scales, *Langmuir*, 2011, **27**, 2484-2491.
48. L. Zhang, X. Zhang, Y. Zhang, J. Hu and H. Fang, *Soft Matter*, 2010, **6**, 4515-4519.
49. W. Wiktoria, M. S. Peter and S. Holger, *Journal of Physics: Condensed Matter*, 2013, **25**, 184005.
50. B. M. Borkent, S. de Beer, F. Mugele and D. Lohse, *Langmuir*, 2010, **26**, 260-268.
51. W. Walczyk and H. Schönherr, *Langmuir*, 2014, **30**, 7112-7126.
52. W. Walczyk, N. Hain and H. Schonherr, *Soft Matter*, 2014, **10**, 5945-5954.
53. X. H. Zhang, N. Maeda and V. S. J. Craig, *Langmuir*, 2006, **22**, 5025-5035.
54. H. An, G. Liu, R. Atkin and V. S. J. Craig, *Acs Nano*, 2015, **9**, 7596-7607.
55. B. Zhao, Y. Song, S. Wang, B. Dai, L. Zhang, Y. Dong, J. Lu and J. Hu, *Soft Matter*, 2013, **9**, 8837-8843.
56. P. Attard and S. J. Miklavcic, *Langmuir*, 2001, **17**, 8217-8223.
57. P. Attard and S. J. Miklavcic, *Langmuir*, 2003, **19**, 2532-2532.
58. P. Attard, *arXiv:1505.02217*, 2015.
59. B. Pittenger, N. Erina and C. Su, *Bruker application note AN128, Rev. B0*, 2012.
60. W. Walczyk, P. Schön, M. and H. Schönherr, *Journal of Physics: Condensed Matter*, 2013, **25**, 184005.
61. C.-W. Yang, Y.-H. Lu and I.-S. Hwang, *Journal of Physics: Condensed Matter*, 2013, **25**, 184010.
62. B. Zhao, X. Wang, Y. Song, J. Hu, J. Lu, X. Zhou, R. Tai, X. Zhang and L. Zhang, *Phys Chem Chem Phys*, 2015, **17**, 13598-13605.
63. X. Zhang, M. H. Uddin, H. Yang, G. Toikka, W. Ducker and N. Maeda, *Langmuir*, 2012, **28**, 10471-10477.
64. S. Lou, J. Gao, X. Xiao, X. Li, G. Li, Y. Zhang, M. Li, J. Sun, X. Li and J. Hu, *Materials Characterization*, 2002, **48**, 211-214.

65. A. Stocco and H. Mohwald, *Langmuir*, 2015, **31**, 11835-11841.
66. X. Wang, B. Zhao, W. Ma, Y. Wang, X. Gao, R. Tai, X. Zhou and L. Zhang, *ChemPhysChem*, 2015, **16**, 1003-1007.
67. B. Song, W. Walczyk and H. Schönherr, *Langmuir*, 2011, **27**, 8223-8232.
68. X. H. Zhang, Z. H. Wu, X. D. Zhang, G. Li and J. Hu, *International Journal of Nanoscience*, 2005, **04**, 399-407.
69. M. A. Hampton and A. V. Nguyen, *J Colloid Interf Sci*, 2009, **333**, 800-806.
70. L. A. Palmer, D. Cookson and R. N. Lamb, *Langmuir*, 2011, **27**, 144-147.
71. G. Vazquez, E. Alvarez and J. M. Navaza, *Journal of Chemical & Engineering Data*, 1995, **40**, 611-614.
72. S. Wang, M. Liu and Y. Dong, *Journal of Physics: Condensed Matter*, 2013, **25**, 184007.
73. R. P. Berkelaar, E. Dietrich, G. A. M. Kip, E. S. Kooij, H. J. W. Zandvliet and D. Lohse, *Soft Matter*, 2014, **10**, 4947-4955.
74. P. Attard, *arXiv:1503.04365*, 2015.

TOC

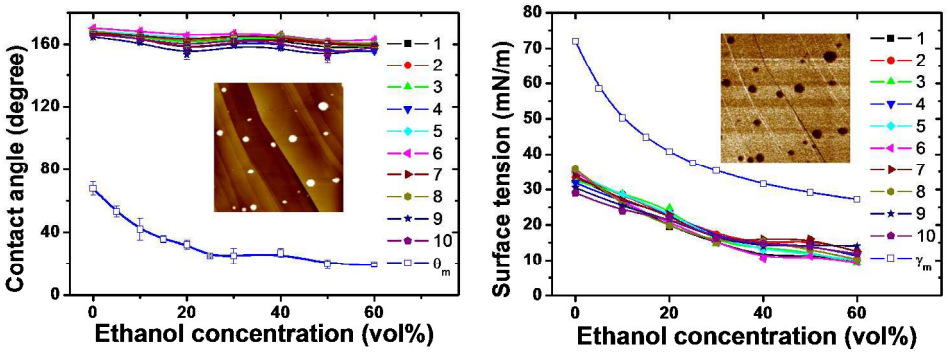

Nanobubbles present larger contact angles and lower surface tensions in ethanol aqueous solutions than those related values at macroscopic scale.